한국기계가공학회지, 제20권, 제7호, pp. 1～7(2021.07) ISSN 1598-6721(Print)
Journal of the Korean Society of Manufacturing Process Engineers, Vol. 20, No. 7, pp. 1~7(2021.07) ISSN 2288-0771(Online)

https://doi.org/10.14775/ksmpe.2021.20.07.001

Evaluation of Insulation Performance and Structural Integrity of an IMO Type C LNG Storage Tank

Heewoo Park*, Jinseong Park**, Jong-Rae Cho**,#
*Korea Register, **Dept. of Mechanical Engineering, Korea Maritime & Ocean University

IMO Type C LNG 저장 탱크의 단열성능 및 구조적 건전성 평가

박희우*, 박진성**, 조종래**,#
*한국선급, **한국해양대학교 기계공학과

(Received 10 June 2021; received in revised form 19 June 2021; accepted 25 June 2021)

ABSTRACT

Restrictions on the emissions of nitrogen oxides, sulfur oxides, carbon dioxide, and particulate matter from marine engines are being tightened. Each of these emissions requires different reduction technologies, which are costly and require many pieces of equipment to meet the requirements. Liquefied natural gas (LNG) fuel has a great advantage in reducing harmful emissions emitted from ships. Therefore, the marine engine application of LNG fuel is significantly increasing in new ship buildings. Accordingly, this study analyzed the internal support structure, insulation type, and fuel supply piping system of a 35 m3 International Maritime Organization C type pressurized storage tank of an LNG-fueled ship. Analysis of the heat transfer characteristics revealed that A304L stainless steel has a lower heat flux than A553 nickel steel, but the effect is not significant. The heat flux of pearlite insulation is much lower than that of vacuum insulation. Moreover, the analysis results of the constraint method of the support ring showed no significant difference. A553 steel containing 9% nickel has a higher strength and lower coefficient of thermal expansion than A304L, making it a suitable material for cryogenic containers.

Key Words : LNG Storage Tank(액화천연가스 저장탱크), Type C tank(C형 탱크), 9% Nickel Steel(9% 니켈강), Insulation(단열), Structural Integrity(구조 건전성)

1. Introduction

Restrictions on the emissions of nitrogen oxides, sulfur oxides, carbon dioxide, and particulate matter from marine engines are being tightened. In particular, nitrogen oxide emission regulations are being intensified.

According to the International Convention for the Prevention of Pollution from Ships (MARPOL) Annex VI of the International Maritime Organization (IMO), the nitrogen oxide limit value was 20% higher for Tier II in 2011 and 80% higher for Tier III in 2016, as compared to that for Tier I in 2000.

Many nitrogen oxide reduction technologies have been developed, such as internal engine

Corresponding Author: cjr@kmou.ac.kr
Tel: +82-51-410-4298, Fax: +82-51-405-4790

modification, direct water injection, humid air motors, fuel water emulsion, exhaust gas recirculation, selective catalytic reduction, and liquefied natural gas (LNG). Most of these technologies meet the Tier II regulations. The technologies that meet the Tier III regulations are selective catalytic reduction and LNG fuel applications[1].

Sulfur oxide regulation is also rapidly improving. The sulfur content of marine fuels globally decreased from 4.5% to 3.5% in 2012 and to 0.5% in 2020. Sulfur oxide reduction technologies involve using a low sulfur fuel oil (marine diesel oil/marine gas oil), applying a scrubber, or using LNG gas fuel[2]. In 2011, MARPOL imposed an energy efficiency standard to reduce greenhouse gas emissions, as stated in Chapter 4 of Annex VI [3]. The IMO included the energy efficiency design coefficient, which is expressed as the mass of carbon dioxide emitted from a ship, as an energy efficiency standard[4]. LNG fuel has a high air fuel ratio and a small amount of carbon, thus reducing carbon dioxide emissions[5].

Hence, the use of LNG as a fuel for marine engines can effectively reduce harmful emissions. Accordingly, nitrogen oxides are reduced by more than 85%, sulfur oxides and particulate matter by 100%, and CO2 emissions by 25%–30%. The use of LNG as a fuel for marine engines is increasing in an effort to effectively reduce all emissions from ships.

According to the International Maritime Legislation[6,7], gas storage tanks are classified as type A, B, or C for LNG-fueled ships. Type A and B tanks operate at pressures below 0.7 bar, and IMO type C tanks are cylindrical pressure slidings that meet the high-pressure vessel criteria of the IGC Code [8]. Type C storage tanks consist of an inner shell and an outer shell and are two-walled cryogenic pressure vessels with a vacuum between two shells [9]. Stainless steel and 5% and 9% nickel steel or aluminum are the general materials used to fabricate cryogenic tanks. Stainless steel is commonly used in small- to medium-sized vessels operating at normal pressure and is widely used in cryogenic piping systems. In particular, Ni steel (9%) is the most economical material used in large-sized vessels where high strength is required.

This study analyzes the internal support structure and insulation type of a 35 m3 IMO type C tank applied to medium- or small-sized engines. Stainless steel A304L and 9% nickel steel A553, which are generally used in cryogenic containers, were analyzed, and the insulation properties between vacuum and pearlite were evaluated.

2. Heat Transfer Analysis of the Tank

2.1 Modeling and boundary conditions

The storage tank consisted of two outer and inner shells and was insulated by vacuum between the shells. The inside of the storage tank was filled with 80% of the tank space with −163 °C LNG under 10 bar pressure, and the outside of the tank was placed under an atmospheric pressure of 1 bar. Two support rings were installed between the two shells. The entire storage tank was supported by two pedestals. The storage tank had an overall length of 12040 mm, an overall diameter of 2400 mm, and a tank capacity of 35 m^3. The structure and shape of the support ring are shown in Fig. 1 and Fig. 2, and the detailed specifications are listed in Table 1.

(a) Overall view

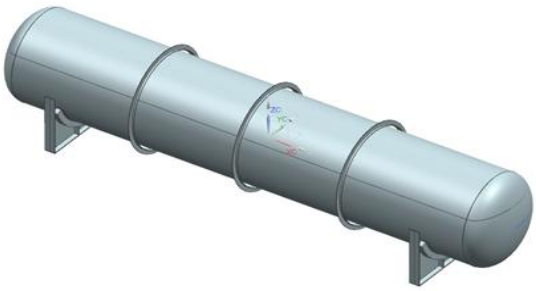

(b) Inner shell

Fig. 1 Structure of the storage tank

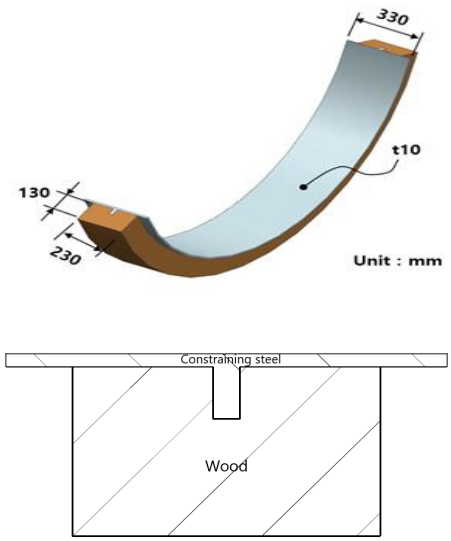

Fig. 2 Structure of the support ring

Table 1 Dimensions of the storage tank

Parts		Dimensions
Outer shell	Length (mm)	12,040
	Diameter (mm)	2,400
	Thickness (mm)	10
Inner shell	Length (mm)	11,488
	Diameter (mm)	2,100
	Thickness (mm)	10
Support ring	Wooden block with T-type constraining steel	
	Height (mm)	150
	Width (mm)	200

The boundary conditions used in the calculation are listed in Table 2[10,11,12]. The exterior of the storage tank was exposed to the atmosphere inside the ship. The surface was under atmospheric pressure (0.1 MPa), and the ambient temperature was 30 °C. Heat transfer from the outer shell to the environment was achieved through natural convection and radiation. The space between the outer and inner shells ignored the convective heat transfer and only considered the radiation heat transfer. The external temperature used to calculate the radiation heat transfer at the outer shell surface was −120 °C, and the external temperature for calculation at the inner shell surface was assumed to be 20 °C. The inside of the tank was filled with cryogenic liquid LNG at a temperature of −163 °C and a pressure of 1.0 MPa. Heat transfer from the inner shell to LNG only considers a convective heat transfer. The entire storage tank was fixed by two pedestals, which were attached to the bottom of the ship and maintained at 25 °C. Stainless steel and 9% nickel steel, which are mainly used in cryogenic containers, were used in this study. The detailed properties are listed in Table 3[13,14,15,16].

Table 2 Boundary conditions

Parts		Conditions
Outer shell	Pressure (MPa)	0.1
	Convection coefficient (W/m^2K)	5
	Ambient temperature (℃)	30
Inner shell	Pressure (MPa)	0.01
	Emissivity coefficient	
	at -120 (℃)	0.0588
	at 20 (℃)	0.0910
Support ring	Pressure (MPa)	1
	Convection temperature(℃)	-163

Table 3 Material properties

Properties	Temp(℃)	A304L	A553
Density (kg/m^3)	-	7900	7860
Coefficient of thermal expansion (10^{-6}/℃)	−196	12.6	8.1
	0	14.7	9.5
Thermal conductivity (W/m℃)	−196	9.0	13
	0	14.27	28.5
Young's modulus (GPa)	−196	205	207
	0	192	186
Yield stress (MPa)	-	215	700

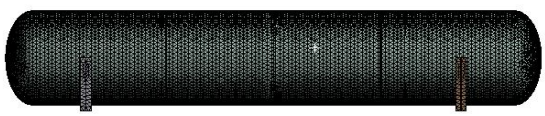

(a) Outer surface of the tank

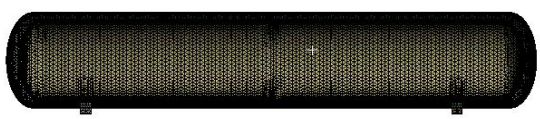

(b) Inner surface of the tank

Fig. 3 Finite element meshes

The calculation of cryogenic tanks was performed stepwise in the heat transfer calculation and structural analysis. The heat transfer calculation was performed to calculate the temperature and heat transfer distribution, and the deformation and stress calculations were performed using thermal boundary conditions. Fig. 3 shows the grids used in the calculations. (a) shows the grids outside the storage tank, and (b) shows the inside structure.

2.2 Heat transfer characteristics

To insulate the inner shell exposed to cryogenic temperatures and the outer shell exposed to high temperatures, the vacuum and pearlite insulation methods were applied, and the heat transfer characteristics were compared and analyzed. Fig. 4 and Fig. 5 show the distribution of temperature and heat flux at the inner shell according to the insulation method and tank material. The results show that the

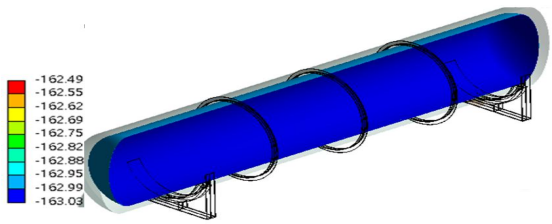

(a) Vacuum insulation

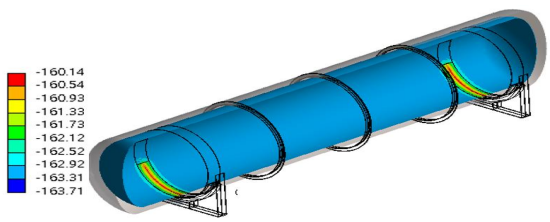

(b) Pearlite powder insulation

Fig. 4 Temperature distribution of the inner shell (A553)

temperature increased around the saddle, and the local heat flux increased.

Fig. 6 shows a comparison of the maximum heat flux for each component of the tank. Insulation is important because the internal LNG is vaporized owing to the heat flux flowing from the outer shell and saddling to the inside. In the case of pearlite insulation (Fig. 6(b)), the heat flux is much smaller than that of the vacuum insulation (Fig. 6(a)). Although the effect of the material was not large, the heat flux slightly increased because the thermal conductivity of A553 was greater than that of A304L.

3. Structural Analysis of the Tank

3.1 Analysis cases and boundary conditions

Table 4 lists the calculation conditions for analyzing the constraining conditions of the support ring. Two supports were installed between the inner and outer shells. One support was bonded to the inner and outer walls. It was divided into three cases according to the constraints of the other support. In

Case 1, the right support was bonded to the inner wall and sliding to the outer wall; Case 2 was bonded to the outer wall and sliding to the inner wall; and Case 3 sliding to the inner and outer walls.

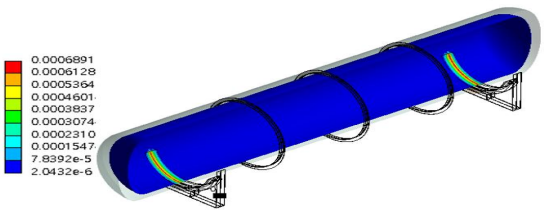

(a) Vacuum insulation

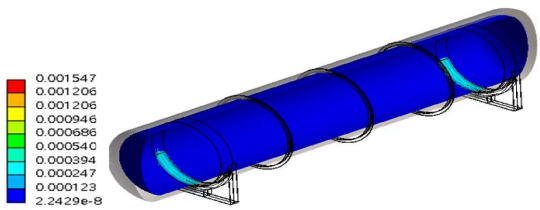

(b) Pearlite powder insulation

Fig. 5 Heat flux(W/mm^2) with insulation methods in the inner shell (A553)

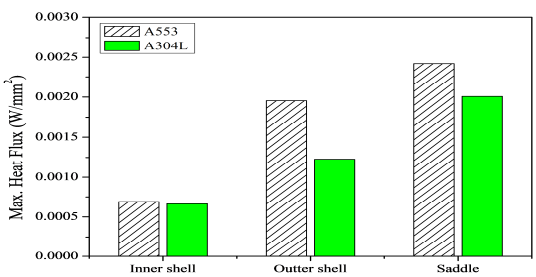

(a) Vacuum insulation

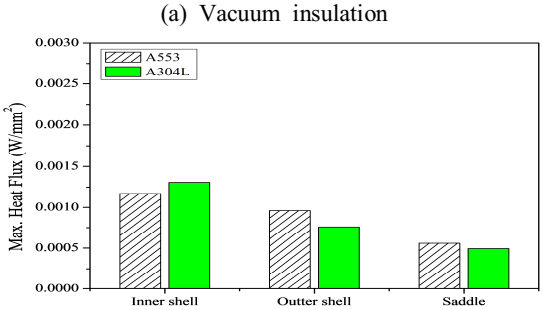

(b) Pearlite powder insulation

Fig. 6 Maximum heat flux in tank components

Table 4 Analysis cases

Analysis case		Conditions
Bonding conditions of support ring	Case 1	Inner bonded and outer both
	Case 2	Outer bonded and inner sliding
	Case 3	Inner bonded and outer sliding

3.2 Structural analysis results

Structural analyses were performed for the A553 and A304L steels in the case of pearlite insulation. Fig. 7 shows the deformation due to pressure (P) + dead load (D) + thermal load (T) according to the constraint conditions of Case 3. The maximum deformation was 5.3 mm. The internal shell deforms downward owing to the weight of the shell steel and LNG inside the tank.

Fig. 7 Deformation of Case 3 in pearlite insulation (A553)

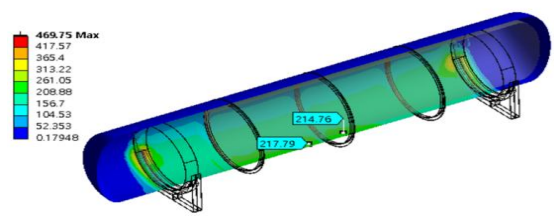

(a) A304L

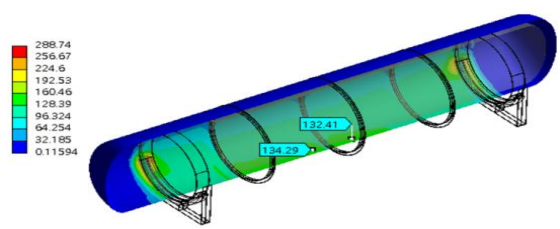

(b) A553

Fig. 8 Equivalent membrane+bending stress distribution of outer shell in pearlite insulation (Case 3)

Fig. 8 shows the equivalent membrane stress of the outer shell in Case 3 under the loading of P+D+T. The maximum stress occurred in the outer shell, where the saddle was attached. There was no significant difference in the temperature distribution between the two shell materials. However, because the linear expansion coefficient of A304L is large, the stress increases in the case of A304L (Fig. 8(a)).

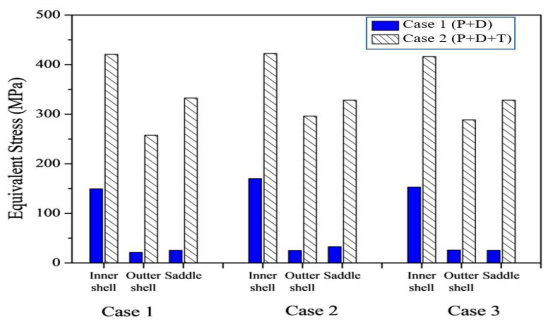

Fig. 9 Equivalent local membrane+bending stress in pearlite insulation w.r.t loading (A553)

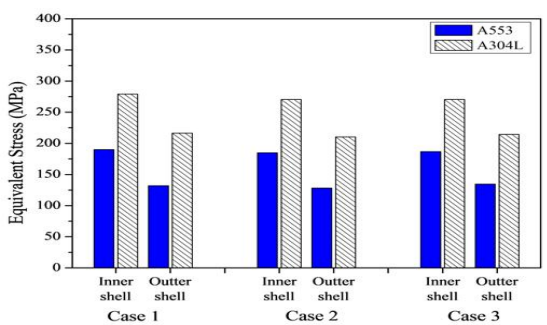

(a) General membrane stress

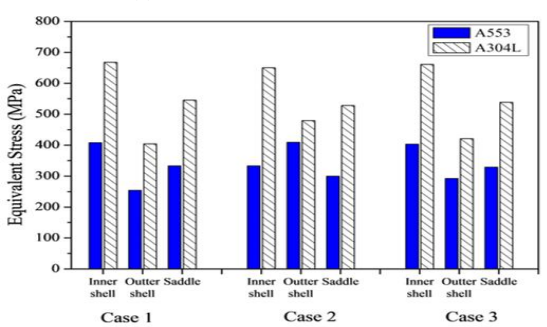

(b) Local membrane+bending stress

Fig. 10 Equivalent stress in pearlite insulation

Fig. 9 shows the stress change according to the loads of P+D and P+D+T. There was no significant difference in the stress among the three analysis cases. However, the stress significantly increased in the case of P+D+T compared to P+D. That is, the thermal stress was the most dominant. In Fig. 10, the stresses of the inner shell were higher than those of the outer shell. The membrane bending stress (Fig. 10(b)) around the saddle was the secondary stress, which is related to the fatigue life of the tank. Because the strength of A553 was much larger than that of A304L, it increased the structural safety and fatigue life. The coefficient of thermal expansion of A553 was much lower than that of A304L, so the thermal stress was reduced.

4. Conclusion

This study analyzes the heat transfer and confirms the structural integrity of a 35 m3 IMO type C tank applied to medium- and small-sized ships. The results are summarized as follows.

1) The calculations were performed by applying stainless steel A304L and 9% nickel A553 materials, which are commonly used in cryogenic containers, to LNG storage tanks under vacuum and pearlite insulation conditions. Stainless steel has a lower heat flux than nickel steel; however, its effect on heat transfer is not significant.
2) Pearlite insulation has a much lower heat flux than vacuum insulation. Because the temperature difference between the cryogenic inner shell and the outer shell is large, radiant heat transfer plays an important role in the heat transfer. Therefore, pearlite insulation that blocks radiant heat transfer is considered to be very advantageous in terms of heat transfer.
3) The constraint conditions of the support ring supporting the inner shell, which were classified to three cases, were analyzed and compared. The

results show no significant difference. The thermal stress was much greater than that due to pressure and dead weight.

4) A553 steel containing 9% nickel has high strength and a low coefficient of thermal expansion, making it a suitable material for cryogenic containers.

References

1. Azzara, A., Rutherford, D., & Wang, H., "Feasibility of IMO Annex VI Tier III implementation using Selective Catalytic Reduction," The International Council on Clean Transportation, Vol. 4, 2014.
2. Adamchak, F. and Adede, A.(2018), "LNG as marine fuel," Retrieved 2020, from https://www.gti.energy/wp-content/uploads/2018/12/7-1-Frederick_Adamchak-LNG17-Paper.pdf.
3. IMO Marine Environment Protection Committee (MEPC), Resolution MEPC.203(62), Amendments to the annex of the protocol of 1997 to amend the international convention for the prevention of pollution from ships, 1973, as modified by the protocol of 1978 relating thereto. IMO, London, 2011.
4. IMO Marine Environment Protection Committee (MEPC), Resolution MEPC.212(63), Guidelines on the method of calculation of the attained energy efficiency design index (EEDI) for new ships. MEPC 63/23. IMO, London, 2012.
5. Jung, R. T., "Recent international development on the technical and operational measures of IMO's CO2 emission control from ships," Journal of the Korean Society for Marine Environmental Engineering, Vol. 14, No. 1, pp. 65–71, 2011.
6. IMO Committee on Maritime Safety (MSC), Resolution MSC.285(86), Interim guidelines on safety for natural gas-fuelled engine installations in ships, IMO, London, 2009.
7. Lamas, M. I., Rodriguez, C. G., Telmo, J. and Rodriguez, J. D., "Numerical analysis of emissions from marine engines using alternative fuels," Polish Maritime Research, Vol. 22, pp. 48–52, 2015.
8. IMO, "International code for the construction and equipment of ships carrying liquefied gases in bulk," 1993.
9. Theotokatos, G., Livanos, G. A., Strantzali, E., Dimitrellou, S., Pagonis, D. N., Peirounakis, D., & Mizithras, P., "Computational investigation of LNG storage tank for open type ferries," In International Congress of the International Maritime Association of the Mediterranean, 2015.
10. "Convective heat transfer coefficients table chart"(2000), https://www.engineersedge.com/heat_transfer/convective_heat_transfer_coefficients__13378.htm (accessed 1, June, 2020)
11. Woods, S. I., Jung, T. M., Sears, D. R., & Yu, J., "Emissivity of silver and stainless steel from 80 K to 300 K: Application to ITER thermal shields," Cryogenics, Vol. 60, pp. 44–48, 2014.
12. "Emissivity of surfaces table-heat transfer", (2000), https://www.engineersedge.com/heat_transfer/emissivity.htm (accessed 1, June, 2020)
13. Avery, R. E., & Parsons, D., "Welding stainless and 9% nickel steel cryogenic vessels," Welding Journal, Vol. 74, pp. 45–50, 1995.
14. "Stainless steel 304L", (2017), https://www.thyssenkrupp-materials.co.uk/stainless-steel-304l-14307.html. (accessed 1, June, 2020)
15. Kern, A., Schriever, U. & Stumfe, J., "Deveopment of 9% Nickel steel for LNG applications", steel research international, Vol. 7, No. 3, pp. 189-194, 2007.
16. Smith, L., & Craig, B., Properties of metallic materials for LNG service, Stainless Steel World, Vol. 13, pp. 27–32, 2001.